Weierstraß-Institut

für Angewandte Analysis und Stochastik

im Forschungsverbund Berlin e. V.

Preprint ISSN 0946 – 8633

Influence of slip on the Rayleigh-Plateau rim instability in dewetting viscous films

Oliver Bäumchen[1], Ludovic Marquant[1], Ralf Blossey[2],

Andreas Münch[3], Barbara Wagner [4], Karin Jacobs[1]

submitted: December 17, 2013

[1] Department of Experimental Physics
Saarland University, Campus
66123 Saarbrücken, Germany
E-Mail: oliver.baeumchen@ds.mpg.de
k.jacobs@physik.uni-saarland.de

[2] Interdisciplinary Research Institute (IRI)
CNRS USR 3078
Parc de la Haute Borne 50
59658 Villeneuve d'Ascq, France
E-Mail: ralf.blossey@iri.univ-lille1.fr

[3] Mathematical Institute
24-29 St Giles'
University of Oxford
Oxford, OX1 3LB, UK
E-Mail: muench@maths.ox.ac.uk

[4] Weierstraß-Institut
Mohrenstraße 39
10117 Berlin, Germany
E-Mail: Barbara.Wagner@wias-berlin.de

No. 1886
Berlin 2013

2010 *Mathematics Subject Classification.* 76A20, 76E17, 76-05.

Key words and phrases. thin-film equations, interfacial slip, contact-line instability.

The authors acknowledge financial support from the German Research Foundation (DFG) within the framework of the priority program SPP 1164 (JA 905/3), graduate school GRK 1276, BA 3406/2, and Matheon.

Edited by
Weierstraß-Institut für Angewandte Analysis und Stochastik (WIAS)
Mohrenstraße 39
10117 Berlin
Germany

Fax: +49 30 2044975
E-Mail: preprint@wias-berlin.de
World Wide Web: http://www.wias-berlin.de/

Abstract

A dewetting viscous film develops a characteristic fluid rim at its receding edge due to mass conservation. In the course of the dewetting process the rim becomes unstable via an instability of Rayleigh-Plateau type. An important difference exists between this classic instability of a liquid column and the rim instability in the thin film as the growth of the rim is continuously fueled by the receding film. We explain how the development and macroscopic morphology of the rim instability are controlled by the slip of the film on the substrate. A single thin-film model captures quantitatively the characteristics of the evolution of the rim observed in our experiments.

One of the best-studied liquid instabilities is the Rayleigh-Plateau instability of a liquid column which, e.g., underlies the break-up of water flowing out of a faucet [1, 2, 3, 4]. Dewetting thin viscous (e.g. polymeric) films display variations of this classic instability and have received ample attention in recent years from both experiment [5, 6, 7, 8, 9, 10, 11] and theory [14, 40, 42]. In thin film flows [15, 16], significant additional physical processes are involved as compared to classical liquid setups: i) in addition to intermolecular forces driving dewetting [37], slip on the substrate [18, 19, 20], viscous and even viscoelastic effects [21] may matter; ii) the retraction of the dewetting front leads to a continuous growth of the rim due to mass conservation while the rim as a whole is pulled across the substrate. The interaction between the liquid in the rim and the substrate is thus of particular importance in these systems. The quantification and the nature of slip is intensively discussed in the literature [22, 23]. Its presence strongly impacts lab-on-a-chip technologies [24], e.g. via the reduction of dispersion and the enhancement of throughput in microfluidic channels [25]. Here we demonstrate the decisive role interfacial slip has for the rim instability in viscous films and link characteristic, optically visible features to microscopic slip at the solid/liquid interface.

Fig. 1 shows an experimental observation of the rim instability as it arises in a dewetting thin film on two types of substrates (upper and lower row). The edge of the receding thin film moves from the left to the right. Its position is given by the dewetted distance $D(t)$. Comparing different films of equal film thickness at identical D ensures identical volume in the rims. A linear geometry has been chosen which bears the advantage that no geometrical restriction on the wavelength of the instability along the rim is imposed, in contrast to equivalent processes at the circumference of holes [10, 11] or rings [26, 27]. Upon advancing, the rim accumulates the dewetted material and in the course of this process passes continuously through three regimes: I) undulations develop along the rim; II) the undulations grow into bulges; III) bulges emerge into fingers ('fingering') whose necks can develop an own Rayleigh-Plateau type instability. In the upper row of Fig. 1, the film passes all three regimes (a) and bulges

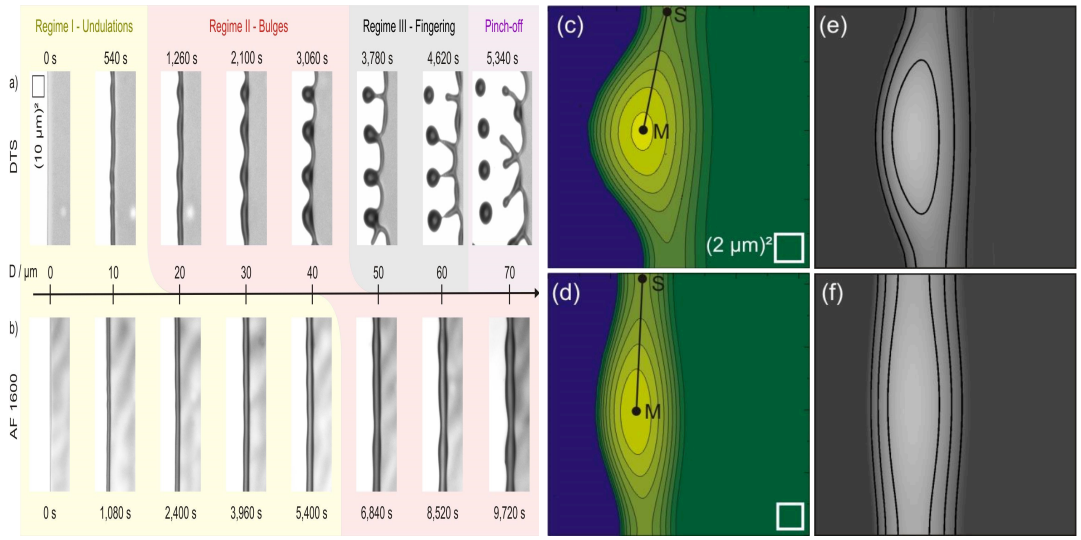

Figure 1: a)-b) Dewetting of a thin viscous film of PS on DTS (top) and on AF1600 (bottom), at $120\,^{\circ}\mathrm{C}$, by retraction of an initially straight front ($13.7\,\mathrm{kg/mol}$, $H = 125(5)\,\mathrm{nm}$) as seen by optical microscopy. A semi-cylindrical liquid rim is formed by the accumulation of liquid material (dark grey). The advance of the front is characterized by the dewetted distance $D(t)$. c)-d) AFM top-view images of a typical bulge on DTS (c) at $D(t)$=$39(2)\,\mu$m and AF1600 (d) at $D(t)$=$45(3)\,\mu$m. e)-f) Top-view 3D numerical simulations for intermediate-slip (e) and no-slip (f) boundary conditions [40], which match the respective experimental bulge morphology. M is the position of the highest point in the contour line plots, S the saddle point. Isoheight lines are set to each $200\,\mathrm{nm}$. In the numerical results, the bulge width has been scaled to one.

exhibit an asymmetric shape (c), whereby, for the same range of dewetted distance, the film in the bottom row does not reach the fingering regime (b) and bulges are symmetric (d).

Both dewetting processes in Fig. 1 feature viscous films of thickness $H \sim 100\,\mathrm{nm}$, but they evolve on two surfaces with different slip properties, as characterized by a slip length b [28]. The slip length represents the length below the solid/liquid interface where the flow velocity profile extrapolates to zero. The substrates are Si wafers (Siltronic) that were hydrophobized either by the preparation of a dodecyl-trichlorosilane (DTS) self-assembled monolayer (SAM) [29] or by spin- or dip-coating an amorphous fluoropolymer layer (AF1600, Aldrich). On AF1600 (bottom row of Fig 1), the liquid films in this study reveal small slip lengths in the range of $b \approx 0.04\,\mu$m, whereas on DTS (upper row in Fig. 1) the exact same films exhibit slip lengths in the range of 1 μm, i.e. $b \gg H$. The slip lengths have been determined using the rim profile analysis method [30, 31, 32, 33] and rationalized by a combined X-ray and neutron reflectivity study [34]. For structural details, surface roughness values and wetting properties of the coatings see Appenix A for tabulated substrate (surface and sub-surface) parameters.

The viscous liquid in this study is unentangled atactic polystyrene (PS, purchased

from PSS). The molecular weights M_w of all experiments are 10.3 or 13.7 kg/mol (polydispersity index $M_\mathrm{w}/M_\mathrm{n} = 1.03$) and, thus, well below the critical value for chain entanglements. Films were prepared by spin-casting a toluene (Selectipur or LiChrosolv, Merck) solution of PS on freshly cleaved mica sheets. Subsequently, the films were floated onto an ultra-pure water (Milli-Q synthesis system, Millipore, organic impurities < 6 ppb, resistance at 25 °C: 18.2 MΩcm) surface and picked up with (freshly cleaned) hydrophobized Si wafers exhibiting a native oxide layer. Dewetting of retracting straight fronts was monitored *in-situ* by optical microscopy on a heating plate (Linkam) as well as *ex-situ* by atomic force microscopy (AFM, ICON and Dimension 3100, Bruker), respectively. The dewetted distance was typically obtained from optical microscopy images; in AFM experiments the dewetted distance can also be calculated from three-dimensional scans of the rim based on volume conservation. Values resulting from both approaches have been checked to be in excellent agreement.

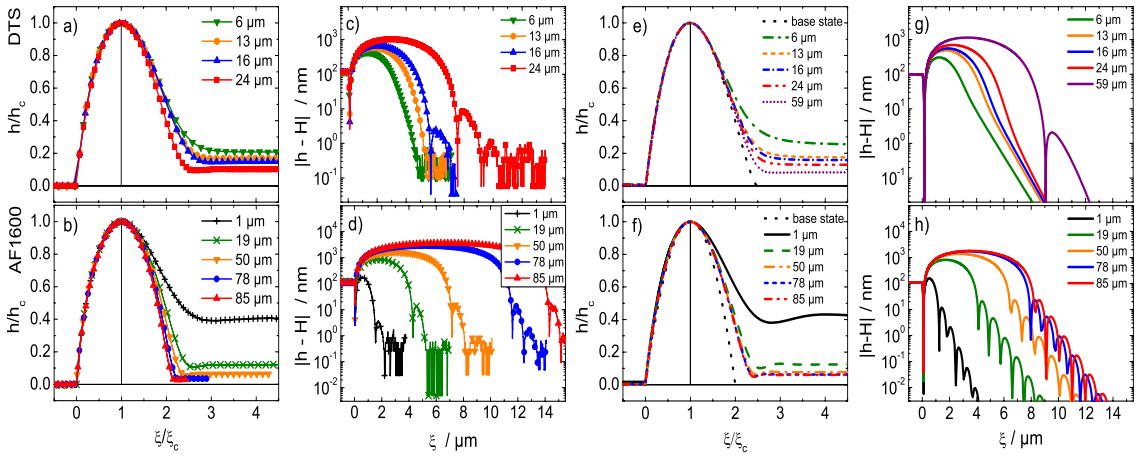

Figure 2: a)-d) AFM scans of rim profiles of straight fronts of a thin film (PS($10.3\,\mathrm{kg/mol}$), $H = 115(5)\,\mathrm{nm}$) on DTS (a,c) at $110\,^\circ\mathrm{C}$ and AF1600 (b,d) at $120\,^\circ\mathrm{C}$, recorded at various travelled distances D as noted in the legend. e)-h) Snapshots of the unperturbed numerical simulations taken at the travelled distance D given by the experiments in a)-d). Normalized h, ξ with the coordinates at maximum h_c, ξ_c illustrate the approach to an asymptotic profile. The vertical straight line helps to visualize the asymmetry between the front and rear of the ridge. On DTS, the semi-logarithmic representation of $|h-H|$ indicates the transition from a monotonously decaying tail to an oscillatory decay. In the presence of slip, both experiments on DTS and numerical calculations of the strong-slip model show a morphological transition of the rim profile. On AF1600, oscillatory profiles are present right from the early stage ($D = 1\,\mu$m) of the dewetting process.

The experimental results can be described by thin-film models that are derived consistently from the Navier-Stokes equations for an incompressible liquid [35, 40]: If the slip length $b = 0$ (or $b \ll H$), the film flow profile is semi-parabolic, and the dynamics corresponds to a weak-slip regime. If $b \gg H$, the dynamics corresponds to plug flow, which arises in two sub-regimes, depending whether extensional stresses in the film

become as important as shear stresses. If only shear stresses matter, the flow regime is called the intermediate-slip regime and otherwise the strong-slip regime. These different regimes can be represented by a single thin-film model for the height profile h, covering the respective limits. For simplicity, we give the model here in 2D, i.e. the cross-section of the height profile $h(x,t)$ over substrate coordinate x and in time t:

$$\begin{aligned} \partial_t h &= -\partial_x \left(h\, u \right), \\ \frac{u}{bh} &= \frac{4\epsilon^2}{h} \left(1 + \frac{h}{2b} \right) \partial_x \left(h \partial_x u \right) \\ &\quad + \left(1 + \frac{h}{3b} \right) \partial_x \left(\partial_{xx} h - \phi'(h) \right). \end{aligned} \tag{1}$$

The weak-slip regime is recovered as the small lubrication parameter $\epsilon \to 0$ in Eq.(1). The strong-slip regime is obtained for the slip length parameter of order of magnitude $b = O(\beta/\epsilon^2)$, the rescaled lateral velocity $u = u^*/\epsilon^2$ and the rescaled time scale $t = \epsilon^2 t^*$ in the asymptotic limit as $\epsilon \to 0$. We also note that the well-known no-slip regime is obtained as a special case of the weak-slip regime as $b = 0$ and the intermediate-slip regime represents the asymptotic limit of the weak- and the strong-slip regime for $1 \ll O(b) \ll O(\epsilon^{-2})$. The simulations of these equations were adapted to the experimental system via the reconstructed effective interface potential $\phi(h)$, given in Ref. [37], as detailed in Appendix A.

For the numerical calculations of the thin-film model we use a 2D (unperturbed) approach as well as full 3D calculations including perturbations along the rim for capturing the morphological details of the bulging. In Fig 1c-f, we present the comparison of our experimental AFM data of the bulge evolution with 3D numerical calculations (using the full equations for wavenumbers that are unstable according to the linear stability theory) based on the corresponding thin-film equations for both substrates, DTS and AF1600. An asymptotic analysis of the thin-film model shows that the no-slip regime leads to symmetric (Fig. 1f) and the intermediate-slip regime to asymmetric bulges (Fig. 1e) [40]. The latter is a consequence of the dependence of the dewetting velocity on the rim width in case of slip: wider sections of the rim retract more slowly than narrower sections [6]. This can easily be observed in Fig. 1a, where the rim instability along with the velocity differences lead to fingering on the slip substrate.

Comparing the time-scales in Fig.1a and b at identical dewetted distance, the dewetting velocity is clearly larger in the slip case (DTS), see Appendix B for a quantification of dewetting velocities and a comparison of morphological features. . Even if we increase the temperature (i.e. decrease the viscosity) in the no-slip case to provoke much higher dewetting velocities than on DTS in Fig. 1a, the morphological features persist and are clearly determined by slippage. The results and the scaling behavior corroborate those previously found for the growth of holes in thin films [33, 36].

Aside from the morphology of the instability and the dewetting dynamics, a third fingerprint is the evolution of the rim shape, in particular how the rim merges into the flat film ahead of its motion. For the DTS substrate, the rim changes from a monotone decay towards the flat film into an oscillatory profile during its evolution at long times

(Fig. 2a,b). By contrast, for AF1600 the rim profile is oscillatory right from the beginning (Fig. 2e,f), a characteristic feature for no-slip substrates [30]. Such a transition from a monotone to an oscillatory rim decay exists only for the strong-slip model and is shown in Fig. 2c,d: The approach to the asymptotic regime depends strongly on the magnitude of b. The asymptotic dynamics of the dewetting rim is generally governed by the intermediate-slip case. In this limit, the rim acquires a limiting profile of asymmetric shape (dotted black line in Fig. 2c) which asymptotically touches down to 0 at $\xi_e \approx 2.5\xi_c$, where ξ is the substrate coordinate in the co-moving frame and ξ_c is the position of the maximum of the rim. The distance $\xi_e - \xi_c$ therefore is a measure of the asymptotic (a)symmetry of the dewetting rim. For the rim profiles on AF1600, the oscillatory behavior is clearly observed in both experiment (Fig. 2e,f) and theory (Fig. 2g,h) and the rim profile in this case converges to a symmetric profile, $\xi_e \approx 2\xi_c$ (Fig. 2g).

We now turn from the rim shape in 2D to its undulation along the rim in 3D, characterized by its wavelength λ, cf. Fig. 3a. The observed wavelength λ first grows in time as a function of dewetted distance $D(t)$ until the film enters the fingering regime (III) for which the wavelength is fixed. The undulatory instability displays a universal characteristics which is demonstrated by plotting the Rayleigh ratio, $C = \lambda/W$ where W is rim width. C is constant, see the insert of Fig. 3b. The reference line in the insert is the theoretical result for C obtained from the intermediate-slip model and is given by $C \approx 2.4$ for the dominant wavelength [40].

The difference between retracting liquid fronts on DTS and AF1600 lies in the rise-time of bulge growth, which is controlled by the interfacial slip. This effect can be estimated by a simple extension, derived in Appendix C, extending a model for liquid rim undulations put forward previously by Brochard-Wyart and Redon (BWR) [42]: A larger slip length imposes a shorter rise-time τ_q, including a shorter rise-time of the dominant mode. In order to compare this theoretical prediction to our experiments, we recorded the lateral amplitude A_x of the instability on both substrates, cf. Fig. 3c. At identical dewetted distance, the growth of A_x is significantly faster on DTS compared to the same viscous film on AF1600. However, the fastest growing wavelength λ for the dominant mode remains unaffected by slip, as validated by the experimental results shown in Fig. 3b.

As mentioned at the beginning, polymer films under shear may also exhibit viscoelastic properties. In the cases we studied, viscoelastic effects in the film are entirely absent as the shear rates $\dot{\gamma}$ are low and the molecular weights are chosen well below the entanglement length. Thus, the longest relaxation times τ_{rel} of the polymers are orders of magnitude shorter than the time frame of the experiments [33]. Therefore, we like to stress the difference of our results to those obtained earlier by Gabriele *et al.* [21]: In the terminology of Gabriele *et al.*, the films are always in a relaxed (or 'mature') regime and do not have to pass through an elastic regime before the undulation instability appears. Finally, we also note that the surface tension of the liquid is uniform and, thus, Marangoni effects are not present. The undulation instability is a purely hydrodynamic effect, whose appearance (but not whose presence) is controlled by the

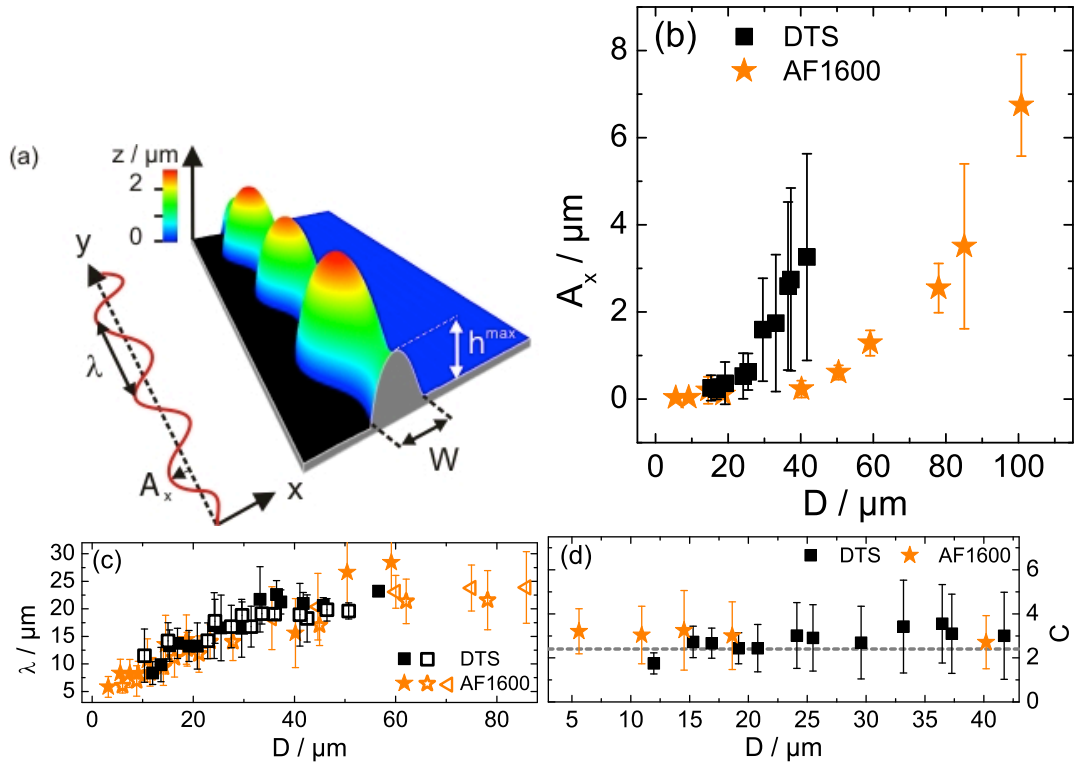

Figure 3: a) AFM image of an undulated rim (10.3 kg/mol at $125\,^{\circ}\mathrm{C}$ on AF1600, $D = 97\,\mu$m, $t = 6360$ s, scan size: $15\,\mu$m x $90\,\mu$m) with parameters characterizing the undulation: rim width W, rim height $h^{\max}$, wavelength λ and lateral amplitude A_x. b) Lateral amplitude A_x of the rim instability in regime I and II determined from AFM images of a PS film (10.3 kg/mol, $H = 115(5)$ nm, $120\,^{\circ}\mathrm{C}$) show distinct differences on DTS and AF1600. c) For the studied film thicknesses $H = 110$–130 nm and molecular weights (10.3 and 13.7 kg/mol), represented by different symbols, the wavelength λ of the instability grows continuously with dewetted distance D and does not depend on the substrate. d) The Rayleigh ratio $C = \lambda/W$ (where W was precisely determined from AFM images, filled symbols) as a function of D for, both, DTS and AF1600 shows a good agreement between experiments and theory (dashed line) [14].

slip length b. The experimental and numerical results presented here are thus valid for all Newtonian liquids, i.e. for Weissenberg numbers $Wi = \tau_{\mathrm{rel}}\dot{\gamma} \ll 1$.

In conclusion, we have shown that the appearance of the Rayleigh-Plateau-type instability of a retracting viscous front is controlled by slip on the substrate. We can predict the characteristic stages of the evolution of the dewetting film within the framework of a single thin-film model. This unified description connects the different morphological transitions seen in our experiments, in particular, (i) for no (or weak) slip: the occurrence of a symmetric rim shape with oscillatory decay and a symmetric instability, (ii) for strong slip: monotone to oscillatory transition of the cross-sectional rim shape towards a profile with asymmetric bulges. Within the experimental error bars,

the characteristic wavelength of the fastest rim undulation λ is unaffected by slip. The rise-time of the bulge growth, however, is lowered with increasing slip and serves as a striking feature for slippage of viscous films.

A general conclusion is that liquid slip not only affects the time scales and, hence, the velocities involved in flow processes or - e.g. in microfluidic channels - the throughput, it also has implications on the spatial morphology. In other words, by monitoring a retracting front of a viscous film through an optical microscope, one can judge whether or not slippage is at work.

A Substrate (surface and sub-surface) parameters and the reconstructed effective interface potential

The simulations of the thin-film equations were adapted to the experimental system via the reconstructed effective interface potential given by [37],

$$\phi(h) = \frac{C_c}{h^8} - \frac{1}{12\pi}\left[\frac{A_c}{h^2} - \frac{A_c - A_{SiO_2}}{(h+d_c)^2} - \frac{A_{SiO_2} - A_{Si}}{(h+d_c+d_{SiO_2})^2}\right], \tag{2}$$

consisting of long-range attractive van der Waals-contributions with Hamaker constants A_i ($i = c$, SiO_2, Si) and a short-range Born-repulsion term of amplitude C_c that penalizes the thinning of the film of initial height H below a minimum of value h^*. The effective potential arises from the contributions of a silicon wafer coated with a native SiO_2 layer of thickness d_{SiO_2} coated by the hydrophobic layer ($c =$ AF1600, DTS) of thickness d_c [38].

	Units	DTS	AF1600
C_c	J/m^6	10^{-81}	$7{\cdot}10^{-81}$
A_c	J	$1.9(3){\cdot}10^{-20}$	$4.3(2){\cdot}10^{-20}$
A_{SiO_2}	J	$2.2(4){\cdot}10^{-20}$	$2.2(4){\cdot}10^{-20}$
A_{Si}	J	$-1.3(6){\cdot}10^{-19}$	$-1.3(6){\cdot}10^{-19}$
d_c	nm	1.5(2)	20(2)
d_{SiO_2}	nm	1.7	1.7
θ_Y	°	67(3)	88(2)
rms	nm	0.13(2)	0.30(1)

The table displays the experimental substrate parameters as a basis for the reconstruction of the effective interface potential $\phi(h)$ used in the 2D (unperturbed) simulations: Hamaker constants A_i for Si, SiO_2, DTS and AF1600 were taken from Refs. [37, 38]. The repulsion coefficients C_c for DTS and AF1600 were calculated to match

the experimentally determined Young's contact angle θ_Y of PS on DTS or AF1600, respectively. The surface tension of PS is 31 mJ.m^{-2} [39]. Layer thicknesses d_i were obtained from nulling ellipsometry measurements (EP^3, Accurion); values for the Young's contact angle were determined from AFM images of PS droplets on the respective substrates in the final stage of dewetting. The root-mean-square roughness rms of the substrate surface, as a characterization of the smoothness and quality of the substrates, was obtained from AFM scans, using a typical scan area of 1 μm x 1 μm and 512 x 512 pixels.

Computationally expensive 3D (perturbed) simulations shown in Fig. 1e,f were run with a set of parameters typical for a liquid on a non-wettable surface for (intermediate) slip (Fig. 1e) and no-slip (Fig. 1f) conditions [40].

B Evaluation of the Dewetting Dynamics and Rim Morphology of Different Dewetting Velocities

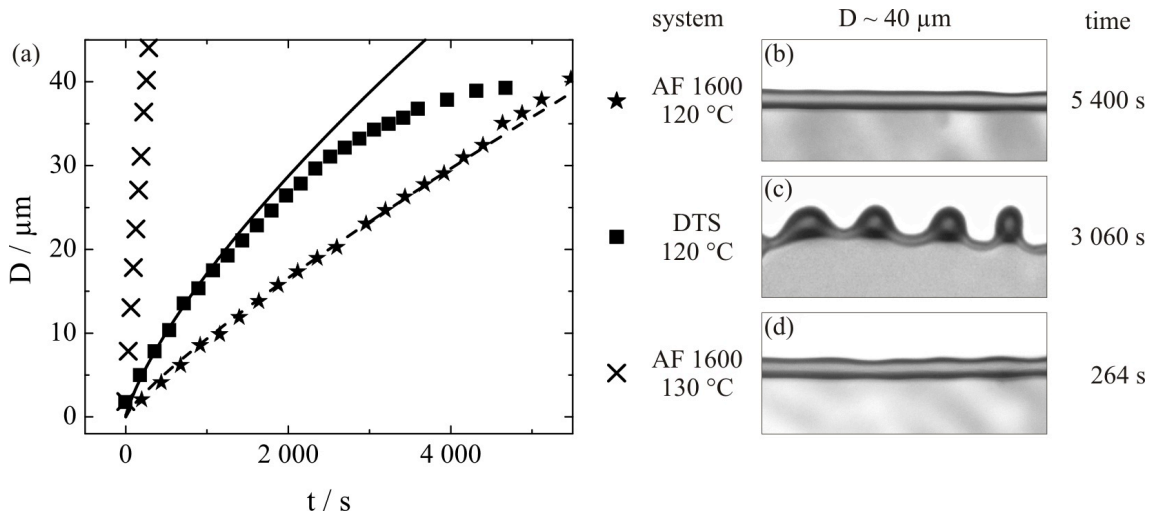

The figure (a) quantifies the evolution of the dewetted distance $D(t)$ for both cases, DTS (rectangles) and AF1600 (stars), shown in the morphological comparison of Fig. 1a,b. On DTS it approaches the asymptotic behaviour $D(t) \sim t^{2/3}$, as expected for the slip-dominated situation [41], before breakdown of the rim into bulges (around 2000 s). In this figure, we also show results from simulations of an unperturbed rim with the strong-slip thin-film equation (straight line) which agree with the experimental data for DTS until the bulging regime is reached. The approach to this growth law strongly depends on the numerical value of b. As we start out with simulations of the strong-slip equation and the obtained growth law corresponds to the intermediate-

slip behaviour, we can conclude that in case of slip the asymptotic behaviour of $D(t)$ is universally governed by the behaviour predicted for the intermediate-slip case. By contrast, for AF1600, $D(t)$ is just slightly sublinear, as expected for the no-slip case [41]. Numerical simulations (dashed line) of an unperturbed rim are in excellent agreement with the experimental data.

At the same temperature and for the same film thickness, the temporal evolution of D on AF1600 (stars) is slow as compared to DTS (rectangles). Increasing the temperature (i.e. decrease the viscosity of the liquid, respectively) for the film on AF1600, a much faster dewetting dynamics can be achieved (crosses, $130\,^{\circ}$C, $10.3\,$kg.mol^{-1}, $H = 115(5)\,$nm). The significant difference in the morphological evolution (b,c,d) of the rim at the same dewetted distance, however, persists and is clearly determined by slippage.

C Extension of the model by Brochard-Wyart and redon (BWR)

In the no-slip case, BWR [42] showed in an approximate calculation that the rise-time τ_q of the undulatory instability, defined by $\dot{u}_q = (-1/\tau_q)u_q$ where u_q is the undulation mode with wavevector q, is given by an expression

$$\frac{1}{\tau_q} = \frac{v^* \theta_Y^3}{3\ell} \frac{1}{1 + \frac{4}{q^2 W^2}} F(q) \tag{3}$$

where

$$F(q) = q \left[-\frac{2}{qW} + \tanh\left(\frac{qW}{2}\right) \right] \tag{4}$$

is the wavevector-dependence of the energy per unit length of a varicose mode of a rim due to Laplace pressure [43]; here, v^* is a characteristic speed and θ_Y the contact angle. Modes with wavevectors q for which the bracket in Eq.(4) is negative will grow, while those for which the bracket is positive will decay exponentially, hence a critical value q_c exists, as is common for a Rayleigh-Plateau instability, and likewise a wavevector of maximal growth, q_m, which determines $\lambda = 2\pi/q_m$. Slip can enter into this theory via the logarithmic prefactor $\ell \equiv \ln(W/b)$ [44] in Eq.(3) for $b \neq 0$.

Consequently, a larger slip length imposes a shorter rise-time τ_q, including a shorter rise-time of the dominant mode.

References

[1] F. Rayleigh, On the instability of jets. Proc. London Math. Soc. **1**, 1 (1878).

[2] J. Plateau, *Experimental and theoretical steady state of liquids subjected to nothing but molecular forces.* (Gauthier-Villars, Paris, 1873).

[3] J. Eggers, Nonlinear dynamics and break-up of free surface flows. Rev. Mod. Phys. **69**, 865 (1997).

[4] J. Eggers and E. Villermaux, Physics of liquid jets. Rep. Progr. Phys. **71**, 036601 (2008).

[5] C. Redon, F. Brochard-Wyart, and F. Rondelez, Dynamics of dewetting. Phys. Rev. Lett. **66**, 715 (1991).

[6] G. Reiter and A. Sharma, Auto-optimization of dewetting rates by rim instabilities in slipping polymer films. Phys. Rev. Lett. **87**, 166103 (2001).

[7] J.-L. Masson, O. Olufokunbi, and P.F. Green, Flow instabilities in entangled polymer thin films. Macromolecules **35**, 6992 (2002).

[8] P. Damman, N. Baudelet, and G. Reiter, Dewetting near the glass transition: transition from a capillary force dominated to a dissipation dominated regime. Phys. Rev. Lett. **91**, 216101 (2003).

[9] B.M. Besancon and P.F. Green, Moving fronts in entangled polymeric films. Phys. Rev. E **70**, 051808 (2004).

[10] A. Sharma and G. Reiter, Instability of Thin Polymer Films on Coated Substrates: Rupture, Dewetting, and Drop Formation J. Coll. Int. Sci. **178**, 383-399 (1996).

[11] S.-H. Choi and B.Z. Newby, Dynamic contact angle in rim instablity of dewetting holes. J. Chem. Phys. **124**, 054702 (2006).

[12] F. Brochard-Wyart and C. Redon, Dynamics of liquid rim instabilities. Langmuir **8**, 2324 (1992).

[13] A. Münch and B. Wagner, Impact of slippage on the morphology and stability of a dewetting rim. J. Phys.: Cond. Matter **23**, 184101 (2011).

[14] J.H. Snoeijer and J. Eggers, Asymptotic analysis of the dewetting rim, Phys. Rev. E **82**, 056314 (2010).

[15] A. Oron, S.H. Davis, and S.G. Bankoff, Long-scale evolution of thin liquid films Rev. Mod. Phys. **69**, 931-980 (1997).

[16] R.V. Craster and O.K. Matar, Dynamics and stability of thin liquid films Rev. Mod. Phys. **81**, 1131-1198 (2009).

[17] R. Seemann, K. Jacobs, and S. Herminghaus, Dewetting patterns and molecular forces: A reconciliation. Phys. Rev. Lett. **86**, 5534 (2001).

[18] P.-G. de Gennes, Wetting: statics and dynamics Rev. Mod. Phys. **57**, 827-863 (1985).

[19] A. Sharma and K. Kargupta, Instability and dynamics of thin slipping films, Appl. Phys. Lett. **83**, 3549-3551 (2003).

[20] O. Bäumchen and K. Jacobs, Slip effects in thin polymer films. J. Phys.: Cond. Matter **22**, 033102 (2010).

[21] S. Gabriele, S. Sclavons, G. Reiter, and P. Damman, Distentanglement time of polymers determines the onset of rim instabilities in dewetting. Phys. Rev. Lett. **96**, 156105 (2006).

[22] L. Bocquet and J.-L. Barrat, Flow boundary conditions from nano- to micro-scales, Soft Matter **3**, 685-693 (2007).

[23] E. Lauga, M.P. Brenner, and H.A Stone, Microfluidics: The No-Slip Boundary, Condition in *Handbook of Experimental Fluid Mechanics*, edited by C. Tropea, A. Yarin J.F. Foss (Springer, New York, 2007), Chap. 19.

[24] T.M. Squires and S.R. Quake, Microfluidics: Fluid physics at the nanoliter scale, Rev. Mod. Phys. **77**, 977 (2005).

[25] D.C. Tretheway and C.D. Meinhart, Apparent fluid slip at hydrophobic microchannel walls, Phys. Fluids **14**, L9 (2002).

[26] J.D. McGraw, J. Li, D.L. Tran, A.-C. Shi, and K. Dalnoki-Veress, Plateau-Rayleigh instability in a torus: formation and breakup of a polymer ring. Soft Matter **6**, 1258 (2010).

[27] A.G. Gonzalez, J.A. Diez, and L. Kondic, Stability of a liquid ring on a substrate, J. Fluid Mech. **718**, 246 (2013).

[28] C.L.M.H. Navier, Mémoire sur les lois du mouvement des fluides. Mem. Acad. Sci. Inst. Fr. **6**, 389 (1823).

[29] M. Lessel, O. Bäumchen, M. Klos, H. Hähl, R. Fetzer, R. Seemann, M. Paulus, and K. Jacobs, Self-assembled silane monolayers: A step-by-step high speed recipe for high-quality, low energy surfaces, arXiv:1212.0998.

[30] R. Fetzer, K. Jacobs, B. Wagner, A. Münch, and T. Witelski, New slip regimes and the shape of dewetting thin liquid films. Phys. Rev. Lett. **95**, 127801 (2005).

[31] O. Bäumchen, R. Fetzer, and K. Jacobs, Reduced interfacial entanglement density affects the boundary conditions of polymer flow. Phys. Rev. Lett. **103**, 247801 (2009).

[32] O. Bäumchen, R. Fetzer, A. Münch, B. Wagner, and K. Jacobs, in *IUTAM Symposium on Advances in Micro- and Nanofluidics*, edited M. Ellero, X. Hu, J. Fröhlich, and N. Adams (Springer, Dordrecht, 2009), p.51. Comprehensive analysis of dewetting profiles to quantify hydrodynamic slip.

[33] O. Bäumchen, R. Fetzer, M. Klos, M. Lessel, L. Marquant, H. Hähl, and K. Jacobs, Slippage and nanorheology of thin liquid polymer films. J. Phys.: Cond. Matter **24**, 325102 (2012).

[34] P. Gutfreund, O. Bäumchen, R. Fetzer *et al.*, Solid surface structure affects liquid order at the polystyrene–self-assembled-monolayer interface. Phys. Rev. E **87**, 012306 (2013).

[35] A. Münch, B. Wagner and T.P. Witelski, Lubrication models with small to large slip lengths. J. Eng. Math. **53**, 359 (2006).

[36] R. Fetzer and K. Jacobs, Slippage of Newtonian Liquids: Influence on the Dynamics of Dewetting Thin Films, Langmuir **23**, 11617 (2007).

[37] R. Seemann, K. Jacobs, and S. Herminghaus, Dewetting patterns and molecular forces: A reconciliation. Phys. Rev. Lett. **86**, 5534 (2001).

[38] O. Bäumchen and K. Jacobs, Can liquids slide? Linking stability and dynamics of thin liquid films to microscopic material properties. Soft Matter **6**, 6028 (2010).

[39] J. Brandrup, E.H. Immergut, and E.A. Grulke, *Polymer Handbook*, 4th ed. (John Wiley & Sons Inc., New York, 1999).

[40] A. Münch and B. Wagner, Impact of slippage on the morphology and stability of a dewetting rim. J. Phys.: Cond. Matter **23**, 184101 (2011).

[41] A. Münch, Dewetting rates of thin liquid films, J. Phys.: Cond. Matter **17**, S309 (2005).

[42] F. Brochard-Wyart and C. Redon, Dynamics of liquid rim instabilities. Langmuir **8**, 2324 (1992).

[43] K. Sekimoto, R. Oguma and K. Kawasaki, Morphological stability analysis of partial wetting. Ann. Phys. **176**, 359 (1987).

[44] F. Brochard-Wyart, P.-G. de Gennes, H. Hervet, and C. Redon, Wetting and slippage of polymer melts on semi-ideal surfaces. Langmuir **10**, 1566 (1994).